# Cytochrome $b_5$ Reductase: Role of the *si*-Face Residues, Proline 92 and Tyrosine 93, in Structure and Catalysis†

Christopher C. Marohnic,‡ Louis J. Crowley,‡ C. Ainsley Davis,‡ Eugene T. Smith,§ and Michael J. Barber*,‡

*Department of Biochemistry and Molecular Biology, College of Medicine, University of South Florida, Tampa, Florida 33612, and Honors College, Florida Atlantic University, Jupiter, Florida 33458*

*Received September 10, 2004; Revised Manuscript Received November 17, 2004*

ABSTRACT: The conserved sequence motif "$RxY^{T}_{S}xx^{S}_{N}$" coordinates flavin binding in NADH:cytochrome $b_5$ reductase (c$b_5$r) and other members of the flavin transhydrogenase superfamily of oxidoreductases. To investigate the roles of Y93, the third and only aromatic residue of the "$RxY^{T}_{S}xx^{S}_{N}$" motif, that stacks against the *si*-face of the flavin isoalloxazine ring, and P92, the second residue in the motif that is also in close proximity to the FAD moiety, a series of rat c$b_5$r variants were produced with substitutions at either P92 or Y93, respectively. The proline mutants P92A, G, and S together with the tyrosine mutants Y93A, D, F, H, S, and W were recombinantly expressed in *E. coli* and purified to homogeneity. Each mutant protein was found to bind FAD in a 1:1 cofactor:protein stoichiometry while UV CD spectra suggested similar secondary structure organization among all nine variants. The tyrosine variants Y93A, D, F, H, and S exhibited varying degrees of blue-shift in the flavin visible absorption maxima while visible CD spectra of the Y93A, D, H, S, and W mutants exhibited similar blue-shifted maxima together with changes in absorption intensity. Intrinsic flavin fluorescence was quenched in the wild type, P92S and A, and Y93H and W mutants while Y93A, D, F, and S mutants exhibited increased fluorescence when compared to free FAD. The tyrosine variants Y93A, D, F, and S also exhibited greater thermolability of FAD binding. The specificity constant ($k_{cat}/K_m^{NADH}$) for NADH:FR activity decreased in the order wild type > P92S > P92A > P92G > Y93F > Y93S > Y93A > Y93D > Y93H > Y93W with the Y93W variant retaining only 0.5% of wild-type efficiency. Both $K_s^{H4NAD}$ and $K_s^{NAD+}$ values suggested that Y93A, F, and W mutants had compromised NADH and $NAD^+$ binding. Thermodynamic measurements of the midpoint potential ($E^{\circ\prime}$, $n = 2$) of the FAD/$FADH_2$ redox couple revealed that the potentials of the Y93A and S variants were ∼30 mV more positive than that of wild-type c$b_5$r ($E^{\circ\prime} = -268$ mV) while that of Y93H was ∼30 mV more negative. These results indicate that neither P92 nor Y93 are critical for flavin incorporation in c$b_5$r and that an aromatic side chain is not essential at position 93, but they demonstrate that Y93 forms contacts with the FAD that effectively modulate the spectroscopic, catalytic, and thermodynamic properties of the bound cofactor.

Cytochrome $b_5$ reductase (c$b_5$r, EC 1.6.2.2)[1] catalyzes the single electron reduction of ferricytochrome $b_5$ to ferrocytochrome $b_5$ using the pyridine nucleotide coenzyme, NADH, as the physiological electron donor. The rate-limiting step in catalysis has been identified as a hydride ion transfer (one proton and two electrons) step from the nicotinamide moiety of NADH to the N5 atom of the FAD prosthetic group of c$b_5$r (*1*). The ability of c$b_5$r and similar flavoproteins to mediate the transfer of reducing equivalents between one and two electron redox centers is fundamental to electron transport events in biological systems. In mammalian species, microsomal and cytosolic c$b_5$r isozymes provide reducing equivalents for a number of physiologically important metabolic processes that include methemoglobin reduction (*2*), fatty acid elongation and desaturation (*3*, *4*), cytochrome P450-mediated hydroxylations (*5*), and cholesterol biosynthesis (*6*).

The structures of the soluble flavin-containing diaphorase domain of rat c$b_5$r and of a c$b_5$r:$NAD^+$ complex have been previously determined to 2.0 and 2.3 Å resolution, respectively (*7*). Residues L25 to G143[2] comprised an antiparallel $\beta$-barrel structure that made the majority of the contacts to the ADP and *si*-face of the isoalloxazine ring of the noncovalently bound FAD prosthetic group. Residues K172−F300 comprised a parallel $\beta$-sheet structure that served as the NADH binding site while also contacting the *re*-face of

† This work was supported by Grants GM 32696 from the National Institutes of Health (M.J.B.) and 9701708 and 9910034V from the American Heart Association, Florida/Puerto Rico Affiliate (M.J.B.).

* To whom correspondence should be addressed. Phone: (813) 974-9702. Fax: (813) 974−7357. E-mail: mbarber@hsc.usf.edu.

‡ University of South Florida.

§ Florida Atlantic University.

[1] Abbreviations: c$b_5$r, cytochrome $b_5$ reductase; c$b_5$, cytochrome $b_5$; FNR, ferredoxin:$NADP^+$ reductase; PDR, phthalate dioxygen reductase; NADH:FR, NADH:ferricyanide reductase; NADH:BR, NADH:cytochrome $b_5$ reductase; $H_4$NAD, 1,4,5,6-tetrahydro-NAD; SDS, sodium dodecyl sulfate; PAGE, polyacrylamide gel electrophoresis; PCR, polymerase chain reaction; IPTG, isopropyl $\beta$-D-thioglucopyranoside; FPLC, fast protein liquid chromatography; TB, terrific broth; $\mu$, ionic strength; CD, circular dichroism; SHE, standard hydrogen electrode.

[2] Amino acid residues are numbered with respect to their position in the sequence of the full-length, membrane-binding form of c$b_5$r (GenBank accession no. P20070).

10.1021/bi048045q CCC: $30.25 
Published on Web 01/25/2005

the FAD. The two domains were hinged by a short 3-stranded $\beta$-sheet comprised of residues P144−V171 that is thought to appropriately orient the surfaces of the two domains around the FAD, thus forming the active site of the enzyme.

Cytochrome $b_5$ reductase shares both sequence and structural similarity with other members of the family of flavoprotein transhydrogenases named for the prototypical member, ferredoxin:NADP$^+$ reductase (FNR, EC 1.18.1.2). Other constituents of the superfamily include nitric oxide synthase (NOS, EC 1.14.13.19), cytochrome P450 oxidoreductase (CYPOR, EC 1.6.2.4), assimilatory nitrate reductase (NR, EC 1.7.1.1) and phthalate dioxygenase reductase (PDR, EC 1.14.12.7). Clusters of highly conserved amino acid residues comprise four key motifs that are interspersed throughout the flavin- and pyridine nucleotide-binding-binding regions of these enzymes (*8*).

The first of these motifs, corresponding to the signature sequence "RxY$^T$$_S$xx$^S$$_N$" ($^{91}$RPYTPVS$^{97}$ in *R. norvegicus* c*b*$_5$r) and shown aligned in Figure 1A for various FNR family members, is one of the most highly conserved of the known flavin-binding motifs, forming contacts with the *si*-face of either FAD or FMN in the crystal structures of many of these enzymes. Based on comparisons of the crystal structures of c*b*$_5$r (*9*), FNR, PDR and NR, Nishida et al. (*10*) proposed a role for two residues, namely the conserved arginine and tyrosine of the "RxY$^T$$_S$xx$^S$$_N$" motif together with an additional serine residue (S99 in porcine c*b*$_5$r), in primarily coordinating flavin-binding through direct hydrogen bonding of the phosphate and ribityl moieties of the cofactor. The same three residues (R63, Y65, and S99) were later mutagenized by Kimura et al. (*11*), who concluded that each had a role in maintaining protein stability and catalysis. Marohnic and Barber demonstrated, using site-directed mutagenesis, that the conserved arginine of the "RxY$^T$$_S$xx$^S$$_N$" motif, corresponding to R91 in rat c*b*$_5$r, was not essential for flavin binding but participated in tethering the ADP moiety of the FAD cofactor to the protein through hydrogen bonding the pyrophosphate oxygens (*12*), disruption of which resulted in significant inhibition of catalytic function through displacement of the ADP moiety of FAD into the NADH-binding cleft (*13*). Recently, the fourth residue of the "RxY$^T$$_S$xx$^S$$_N$" motif in porcine c*b*$_5$r, T66, was shown to modulate the formation and stability of the NAD$^+$-FAD$^-$ semiquinone complex during NADH turnover (*14*). The positions of the residues comprising the "RxY$^T$$_S$xx$^S$$_N$" motif in relation to the FAD of rat c*b*$_5$r are illustrated in Figure 1B.

To systematically assess the structural and functional contributions of the hydrogen bonding, hydrophobic interactions and van der Waals contacts formed between the second (P92) and third (Y93) residues in the motif and the *si*-face of the FAD cofactor of rat c*b*$_5$r diaphorase domain, site-directed mutagenesis was used to generate a series of P92- and Y93-substituted variants. For the Y93 variants, substitutions were engineered to selectively maintain or eliminate the hydrogen bonding, $\pi-\pi$ interactions and hydrophobic interactions with the *si*-face of the isoalloxazine ring. As a proximity control, the nonconserved second residue of the "RxY$^T$$_S$xx$^S$$_N$" motif, P92, was also subjected to mutagenic analysis, since it has also been shown to be within 5 Å of the *si*-face of the cofactor.

**A**

| Enzyme | RxY$^T$$_S$xx$^S$$_N$ | Accession #/Reference |
|---|---|---|
| cytochrome $b_5$ reductase | $^{91}$RPYTPVS$^{97}$ | NP_620232 / [32] |
| NADH:nitrate reductase | $^{722}$RAYTPPS$^{728}$ | P23312 / [33] |
| ferredoxin:NADP$^+$ reductase | $^{139}$RLYSIAS$^{145}$ | P10933 / [34] |
| cytochrome P450 reductase | $^{454}$RYYSIAS$^{460}$ | P16435 / [35] |
| nitric oxide synthase | $^{1178}$RYYSISS$^{1184}$ | P29475 / [36] |
| phthalate dioxygenase reductase | $^{51}$RNYSLSN$^{57}$ | Q05182 / [37] |
| methionine synthase reductase | $^{478}$RPYSCAS$^{484}$ | Q9UBK8 / [38] |
| sulfite reductase | $^{386}$RLYSIAS$^{392}$ | P38038 / [39] |
| flavohemoglobin | $^{204}$RQYSLTR$^{210}$ | P24232 / [40] |
| c*b*$_5$/c*b*$_5$r fusion protein | $^{289}$KPYTPVS$^{295}$ | NP_596918 / [41] |
| electron transfer flavoprotein | $^{56}$RCYSITS$^{62}$ | BAA12809 / Fukumori 1996* |
| naphthalene dioxygenase reductase | $^{142}$RPYSMAG$^{148}$ | AAD02134 / [42] |
| phenol hydroxylase | $^{149}$RAFSLAN$^{155}$ | AAA25944 / [43] |
| NADPH:flavin reductase | $^{58}$RPFSMAS$^{64}$ | AAN83224 / [44] |
| CDP-glucose 4,6-dehydratase | $^{143}$RSYSIAN$^{147}$ | P26395 / [45] |
| p-cymene monooxygenase reductase | $^{159}$RSYSFAN$^{165}$ | AAB62300 / [46] |
| xylene monooxygenase reductase | $^{160}$RSYSFAT$^{166}$ | AAB70826 / Gilbert 1997* |
| nitrotoluene monooxygenase reductase | $^{161}$RSYSFSA$^{167}$ | AAC38360 / [47] |
| dihydroquinoline monooxygenase reductase | $^{155}$RSYSPSS$^{161}$ | CAA73201 / [48] |
| methane monooxygenase reductase | $^{159}$RSYSPAN$^{165}$ | P22868 / [49] |
| anthrinilate dioxygenase reductase | $^{154}$RSYSFAN$^{160}$ | AAC34815 / [50] |
| toluate dioxygenase reductase | $^{153}$RAYSFSS$^{159}$ | AAD31449 / Benjamin 1999* |
| benzoate dioxygenase reductase | $^{166}$RSYSFSS$^{172}$ | P07771 / [51] |
| halobenzoate dioxygenase reductase | $^{152}$RAYSYSS$^{158}$ | Q51603 / [52] |
| NADH:quinone reductase I | $^{222}$KAYSLAS$^{228}$ | Q9Z723 / [53] |
| *M. loti* unknown flavoprotein | $^{168}$RLYLVST$^{174}$ | NP_107088 / [54] |
| *Halobacterium sp. NRC-1* unknown protein | $^{51}$RYYTLSS$^{57}$ | NP_279534 / [55] |
| *Xanthobacter* hypothetical reductase | $^{142}$RAYSVAN$^{148}$ | CAA09916 / [56] |

*Direct GenBank submissions

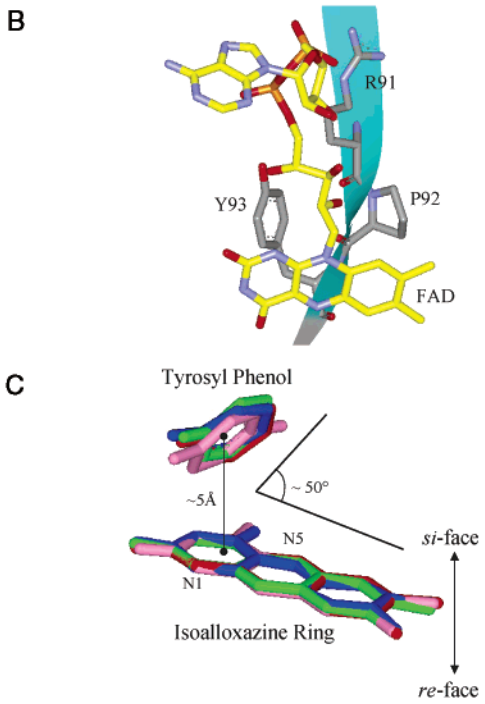


FIGURE 1: (A) Multiple sequence alignment of the "RxY$^T$$_S$xx$^S$$_N$" motif within the primary sequences of various members of the flavin transhydrogenase superfamily. The highly conserved *si*-face aromatic residue, equivalent to Y93 of c*b*$_5$r, is shown in bold type face. (B) Rendering of the first three residues of the "RxY$^T$$_S$xx$^S$$_N$" motif in the structure of rat c*b*$_5$r (*7*) facing the *re*-side of the flavin cofactor. The peptide backbone is drawn in ribbon configuration while the R91, P92, and Y93 side-chain atoms, along with the FAD, are drawn in stick configuration with CPK coloring, except FAD carbons, which are colored yellow. (C) Superposition of lumiflavin and the *si*-face tyrosine atoms from the structures of FNR (blue) (*31*), NR (green) (*28*), CYPOR (pink) (*29*) and c*b*$_5$r (red) (*7*), drawn in stick configuration.

## MATERIALS AND METHODS

*Materials.* Oligonucleotide primers were obtained from Integrated DNA Technologies (Coralville, IA). *Pfu* Turbo Polymerase as well as *Epicurian coli* BL21(DE3)-RIL cells were obtained from Stratagene (La Jolla, CA). Restriction enzymes were purchased from New England Biolabs (Bev-

Table 1. Mutagenic Oligonucleotide Primers Used in the Generation of the Various P92 and Y93 c$b_5$r Variants[a]

| Variant | Primer Sequence (5'→3')[#] | Restriction Site |
|---|---|---|
| P92A | GGC AAC TTG GTC ATT CGT ***GCC*** TAC ACC CCT GTG | - *Bsm*FI |
| P92G | GGC AAC TTG GTC ATT CGT ***GGC*** TAC ACC CCT GTG | - *Bsm*FI |
| P92S | GGC AAC TTG GTC ATT CGT ***TCC*** TAC ACC CCT GTG | - *Bsm*FI |
| Y93A | AAC TTG GT*G* ATT CGT CCC **GCG** ACC CCT GTG TCT | +*Hin*FI |
| Y93D | AAC TTG GT*G* ATT CGT CCC **GAC** ACC CCT GTG TCT | +*Hin*FI |
| Y93F | AAC TTG GT*G* ATT CGT CCC **TTT** ACC CCT GTG TCT | +*Hin*FI |
| Y93H | AAC TTG GT*G* ATT CGT CCC **CAC** ACC CCT GTG TCT | +*Hin*FI |
| Y93S | AAC TTG GT*G* ATT CGT CCC **TCC** ACC CCT GTG TCT | +*Hin*FI |
| Y93W | AAC TTG GT*G* ATT CGT CCC **TGG** ACC CCT GTG TCT | +*Hin*FI |
| Wild-type | GGC AAC TTG GTC ATT CGT CCC TAC ACC CCT GTG TCT | |
| Amino acid | N- G N L V I R **P** **Y** T P V S -C | |

[a] Nucleotides shown in bold encode the mutated residue. Silent mutations, shown in italics, resulted in the addition (+) or elimination (−) of the indicated restriction site.

Table 2. NADH:FR and NADH:BR Kinetic Constants Obtained for the Various c$b_5$r P92 and Y93 Mutants

| | NADH:FR activity | | | | NADH:BR activity | | |
|---|---|---|---|---|---|---|---|
| variant | $k_{cat}$ ($s^{-1}$) | $K_m^{NADH}$ ($\mu$M) | $K_m^{Fe(CN)_6}$ ($\mu$M) | $k_{cat}/K_m^{NADH}$ ($s^{-1}$ $M^{-1}$) | $k_{cat}$ ($s^{-1}$) | $K_m^{cytb_5}$ ($\mu$M) | $k_{cat}/K_m^{cytb_5}$ ($s^{-1}$ $M^{-1}$) |
| wild-type | 800 ± 16 | 6.0 ± 0.5 | 7.1 ± 1.0 | (1.3 ± 0.1) × $10^8$ | 400 ± 33 | 13 ± 2 | (3.1 ± 0.1) × $10^7$ |
| P92S | 880 ± 30 | 7.7 ± 1.1 | 7.8 ± 1.6 | (1.2 ± 0.2) × $10^8$ | 315 ± 12 | 12 ± 1 | (2.6 ± 0.1) × $10^7$ |
| P92A | 517 ± 18 | 4.8 ± 0.8 | 7.4 ± 1.0 | (1.1 ± 0.2) × $10^8$ | 320 ± 10 | 15 ± 1 | (2.1 ± 0.1) × $10^7$ |
| P92G | 467 ± 28 | 6.5 ± 0.9 | 8.0 ± 1.0 | (7.2 ± 0.2) × $10^7$ | 335 ± 21 | 12 ± 1 | (2.8 ± 0.1) × $10^7$ |
| Y93F | 483 ± 16 | 6.7 ± 0.2 | 6.6 ± 0.3 | (7.2 ± 0.6) × $10^7$ | 295 ± 33 | 11 ± 1 | (2.7 ± 0.1) × $10^7$ |
| Y93A | 200 ± 15 | 7.3 ± 0.8 | 8.6 ± 0.4 | (2.7 ± 0.2) × $10^7$ | 57 ± 5 | 14 ± 1 | (4.1 ± 0.1) × $10^6$ |
| Y93S | 133 ± 12 | 3.8 ± 0.3 | 5.8 ± 1.3 | (3.5 ± 0.1) × $10^7$ | 32 ± 4 | 12 ± 1 | (2.7 ± 0.1) × $10^6$ |
| Y93D | 83 ± 12 | 4.9 ± 0.5 | 8.3 ± 2.0 | (1.7 ± 0.3) × $10^7$ | 14 ± 2 | 10 ± 2 | (1.4 ± 0.1) × $10^6$ |
| Y93H | 83 ± 10 | 8.8 ± 1.2 | 8.3 ± 1.5 | (9.4 ± 2.5) × $10^6$ | 27 ± 4 | 10 ± 1 | (2.7 ± 0.1) × $10^6$ |
| Y93W | 33 ± 10 | 54 ± 8 | 6.8 ± 2.0 | (6.1 ± 1.8) × $10^5$ | 19 ± 2 | 11 ± 1 | (1.7 ± 0.1) × $10^6$ |

erly, MA). Tryptone and yeast extract were obtained from EM Science (Gibbstown, NJ). IPTG was obtained from RPI (Mt. Prospect, IL). Reagents for bacterial culture, protein purification, and chemical assays including NADH, $NAD^+$, riboflavin, FAD, and $K_3Fe(CN)_6$ were obtained from Sigma Chemical Co. (St. Louis, MO). Ni−NTA agarose and kits for plasmid preparation and agarose gel extraction were purchased from Qiagen Inc. (Valencia, CA).

*Site-Directed Mutagenesis.* c$b_5$r mutants were constructed using whole vector PCR as described previously (*12*) whereby the four histidine-tagged c$b_5$r expression construct was specifically mutagenized using complimentary oligonucleotide primers (30−35 mers) as listed in Table 1. The fidelity of the mutant constructs were verified by nucleotide sequencing in both the forward and reverse directions. Positive constructs were then used to transform competent *E. coli* BL21(DE3)-RIL cells.

*Cell Culture and Protein Purification. E. coli* BL21(DE3)-RIL cells harboring the $pH_4cb_5r$ or mutant constructs were grown aerobically in TB media supplemented with riboflavin (100 $\mu$M) overnight at 37 °C. Recombinant protein expression and purification were carried out as described previously (*12*). The soluble heme-containing domain of rat c$b_5$ was prepared as previously described by Beck-von Bodman (*15*). Wild-type and mutant c$b_5$r concentrations were estimated spectrophotometrically. For the wild-type enzyme, an extinction coefficient of $A_{461\ nm} = 10.6\ cm^{-1}\ mM^{-1}$ was used. The molar extinction coefficient for each of the mutant enzymes was determined by comparison of the flavin visible absorbance spectra prior to and following protein denaturation using $A_{450nm} = 11.3\ cm^{-1}\ mM^{-1}$ to quantitate free FAD. Extinction coefficients of the mutant proteins, listed in Table 2, were used for all subsequent quantifications. SDS-polyacrylamide gel electrophoresis was performed as described by Laemmli (*16*).

*Spectroscopy.* All spectroscopic measurements utilized oxidized enzymes in 10 mM potassium phosphate buffer, containing 0.1 mM EDTA, pH 7.0. UV/visible absorbance spectra were obtained using a Hewlett-Packard (Agilent Technologies, Palo Alto, CA) 8453 diode-array spectrophotometer. UV and visible CD spectra were obtained using a JASCO (Easton, MD) J710 spectropolarimeter as described previously (*12*). All spectra were corrected for the appropriate buffer contributions and are expressed in terms of molar ellipticities ($M^{-1}\ cm^{-1}$). Fluorescence excitation and emission spectra were obtained using a RF5301PC spectrofluorimeter (Shimadzu Scientific Inst. Inc., Columbia, MD).

Spectral binding constants, $K_s$, were determined using differential spectroscopy as previously described by Ma-

rohnic et al. (*17*). $H_4$NAD was synthesized as described by Murataliev et al. (*18*).

*Enzyme Activities.* NADH:FR and NADH:BR activities were determined at 25 °C under conditions of constant ionic strength and pH as previously described (*12*) in 116 mM MOPS buffer, containing 0.1 mM EDTA, pH 7.0 ($\mu = 0.05$). Initial rate data were analyzed using the software "ENZFIT" (Elsevier Biosoft, Ferguson, MO) to yield apparent $k_{cat}$ and $K_m$ values.

*Thermostability Measurements.* Thermal stability profiles for both the wild-type and mutant proteins were determined by monitoring both the release of the FAD prosthetic group, indicated by the increase in intrinsic flavin fluorescence, and the loss of NADH:FR activity as previously described (*19*). Protein samples (18−20 $\mu$M FAD) in 50 mM phosphate buffer, containing 0.1 mM EDTA, pH 7.5, were initially incubated at 0 °C for 5 min followed by successive 5-min incubations at 5−10 °C intervals. Aliquots were removed at the end of each temperature change, diluted into ice-cold buffer and assayed for both NADH:FR activity and intrinsic flavin fluorescence. The samples were also analyzed at the conclusion of the inactivation profile and the average of the values was plotted relative to the initial enzyme activity at 0 °C.

*Oxidation−Reduction Potentials.* For the direct determination of the flavin midpoint potentials of wild-type c$b_5$r and the various mutant constructs by cyclic voltammetry, an anaerobic microcell apparatus containing a pyrolitic graphite working electrode, a Ag/AgCl reference electrode, and a platinum counter electrode, was constructed for use with a Bioanalytical Systems Inc. (West Lafayette, IN) model Epsilon-EC potentiostat as described previously (*19*). Protein samples (20 $\mu$L) were prepared at 500 $\mu$M concentration in 100 mM phosphate buffer containing 0.1 mM EDTA and were made anaerobic by extensive flushing with oxygen-free argon prior to use.

Flavin midpoint potentials were also determined by dye equilibration potentiometry using the method of Massey (*20*) whereby xanthine (30 $\mu$M) and xanthine oxidase (50 nM) were used to reduce a mixture of enzyme (40 $\mu$M FAD) and phenosafranine (15 $\mu$M) in 100 mM phosphate buffer, containing 0.1 mM EDTA, pH 7.0 first made anaerobic by repeated evacuation and flushing with oxygen-free argon. Benzyl viologen (6 $\mu$M) and methyl viologen (1 $\mu$M) were included to facilitate equilibration of the system. Visible absorbance spectra were collected over the course of each 3−6 h determination. Flavin reduction was monitored at 410 nm while phenosafranine reduction was monitored at 530 nm. $E^{\circ\prime}$ values were calculated by analysis of the plot of potential (mV) versus $(\log [ox]/[red])_{FAD}$ using the published midpoint potential of phenosafranine of −252 mV (*20*). Oxidation−reduction potentials are reported with reference to the SHE and are considered accurate to ±5 mV.

## RESULTS

*Mutagenesis, Expression, and Protein Purification.* Mutant constructs encoding the different c$b_5$r variants, P92A, G, and S together with Y93A, D, F, H, S, and W, which corresponded to the second and third residues in the conserved "$RxY^{T}_{S}xx^{S}_{N}$" sequence motif, respectively, were generated through directed mutagenesis of the original four-histidine tagged c$b_5$r construct. Nucleotide sequencing confirmed the fidelity of each construct and each of the mutant proteins was subsequently expressed in the *E. coli* strain BL21(DE3)-RIL and purified by Ni-chelate chromatography and gel filtration FPLC. Evaluation of the expression yields of the various mutants indicated that while the three P93 variants were expressed at levels comparable to that of the wild-type domain, the yields of the six Y93 mutants were highly variable. Conservative mutants such as Y93F were produced at wild-type levels while some of the radical mutants, including Y93D and Y93H, generated significantly decreased amounts of protein that were relatively unstable and highly prone to aggregation and precipitation. However, all nine mutants were purified to apparent homogeneity as evident by the presence of single protein bands following SDS−PAGE analysis of selected mutants as shown in Figure 2. The nine c$b_5$r variant apoproteins were of similar molecular mass to that of the native enzyme while MALDI-TOF analyses revealed the presence of a characteristic peak in the low mass region of each spectrum with a *m*/*z* of 792, indicative of the presence of FAD as the sole prosthetic group. These findings suggested that neither P92 nor Y93 provided backbone or side-chain contacts that were essential for the stable incorporation of oxidized FAD into any of the c$b_5$r variants.

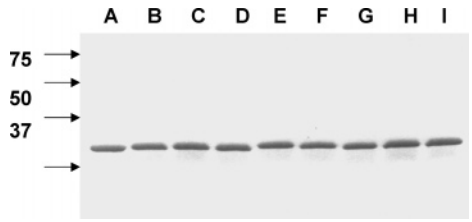


FIGURE 2: SDS−PAGE analysis of selected P92 and Y93 c$b_5$r mutant proteins. Purified proteins (2 $\mu$g each protein) obtained from the final FPLC purification step of both the wild-type c$b_5$r and the individual P92 and Y93 mutant constructs were resolved on a 15% polyacrylamide gel: lane A, wild-type c$b_5$r; lane B, P92A; lane C, P92S; lane D, Y93A; lane E, Y93F; lane F, Y93H; lane G, Y93W; lane H, Y93S; lane I, Y93D. The arrows indicate the positions of selected molecular weight markers with the indicated molecular masses (kDa).

*Spectroscopy.* UV/visible absorbance spectra were obtained for oxidized samples of wild-type c$b_5$r and each of the mutants, as presented in Figure 3. The P92A, P92S, P92G, and Y93W variants each exhibited spectra comparable to that of the wild-type enzyme with an aromatic absorption maximum observed at 270 nm in the UV region of the spectrum, and a peak at 461 nm with an associated pronounced shoulder in the range of 485−500 nm in the visible region of the spectrum, attributable to protein-bound flavin. Each of the remaining Y93-substituted variants, however, exhibited perturbed visible absorbance spectra with varying degrees of blue-shift. The most dramatically shifted spectrum was that of the Y93H variant with an associated $\lambda_{max}$ of 449 nm, a shift of 12 nm compared to the wild-type enzyme. The visible absorption maxima of the remaining mutants were perturbed to different extents with the Y93F, Y93A, Y93S and Y93D mutants exhibiting maxima at 460, 458, 454, and 452 nm, respectively. Blue-shifts in the visible absorbance spectra of flavoproteins have previously been attributed to changes in the hydrophilicity of the flavin environment near the N(5) locus of the isoalloxazine ring

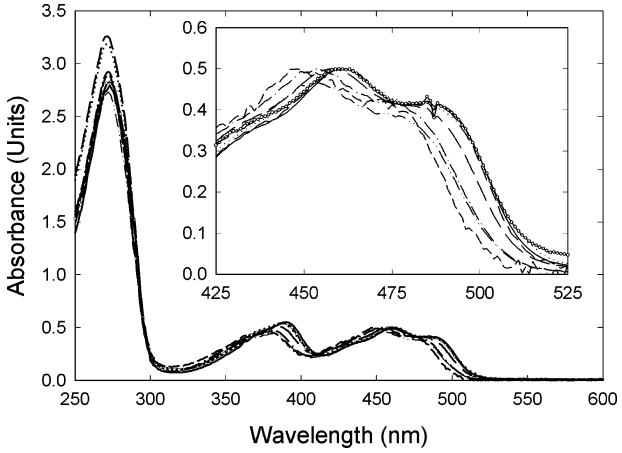


FIGURE 3: UV/visible absorbance spectra of the various P92 and Y93 c$b_5$r mutant proteins. Oxidized samples of wild-type and the various P92 and Y93 c$b_5$r variants were prepared at equivalent FAD concentrations (50 $\mu$M) in 10 mM phosphate buffer, containing 0.1 mM EDTA, pH 7.0. Individual spectra correspond to wild type (—), P92A (-○-), Y93A (— — —), Y93F (— — —), Y93H (- - -), Y93W (•••), Y93S (-•-), and Y93D (-••-), respectively. The spectra of P92S and P92G are not displayed since they were comparable to those of P92A and wild-type c$b_5$r.

(*12*, *21*, *22*). Substitution of Y93 with either alanine or phenylalanine was expected to increase the hydrophobicity near the flavin, but the spectra of the Y93A and Y93F variants were less perturbed than those of the Y93H, Y93D, and Y93S variants which were expected to have increased hydrophilicity at position 93. These findings suggested that the visible absorption spectrum of oxidized c$b_5$r was very sensitive to the presence of polar residues, whether charged or uncharged, at position 93, but not at position 92.

To evaluate the secondary structural content of each of the mutant enzymes, CD spectra were recorded in the UV wavelength range (190−300 nm). As shown in Figure 4A (left panel), all of the c$b_5$r variants exhibited positive CD from 190 to 210 nm and negative CD from 210 to 250 nm with all the spectra retaining both positive and negative intensities very similar to that of the wild-type domain. The absence of any significant differences between the spectra of the wild-type and mutant proteins suggested the conservation of secondary structure and that none of the P92 or Y93 residue substitutions had any deleterious effects on the folding of the flavin-binding $\beta$ barrel.

In contrast to the UVCD spectra, all the Y93 mutations were observed to have a profound influence on the corresponding visible CD spectra. Circular dichroism measurements were performed in the near-UV/visible range (300−600 nm) in order to probe the effects of the various mutations on both flavin conformation and polarity of the prosthetic group microenvironment. As shown in Figure 4A (right panel), the spectra of the Y93A, Y93D, Y93H, Y93S, and Y93W mutants were significantly perturbed when compared to that of wild-type c$b_5$r, while the spectra of the P92A, G, and S variants were comparable to that of wild-type enzyme. The positive and negative maxima of the spectrum of the wild-type enzyme, occurring at approximately 400 and 460 nm, respectively, were of similar intensity but were shifted to 375 and 450 nm, respectively, for the Y93H variant. For the spectra of the Y93A and Y93S variants, the CD maxima were shifted to shorter wavelength and were also of decreased intensity when compared to the corresponding transitions

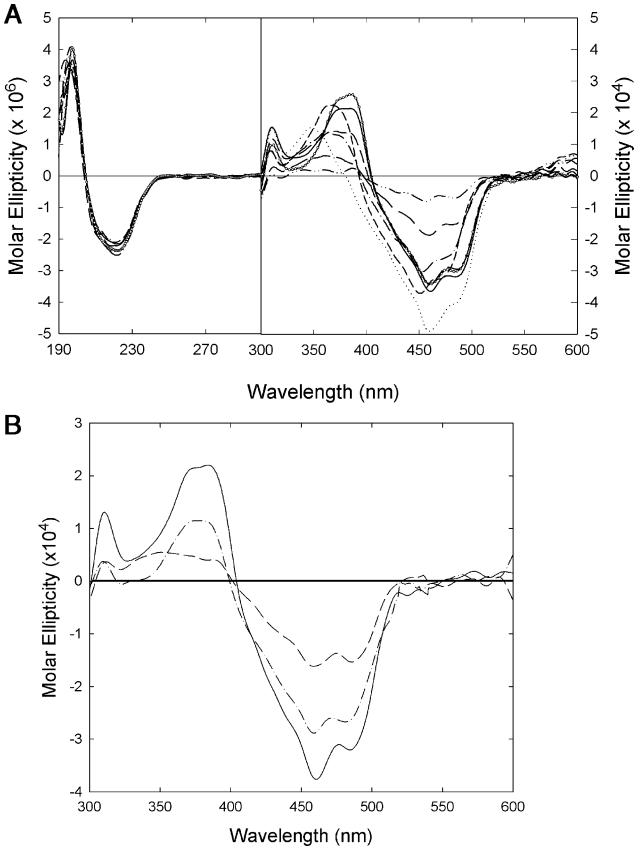


FIGURE 4: UV and visible CD spectra of the various P92 and Y93 mutants c$b_5$r proteins. (A) Left panel: Oxidized samples of wild-type c$b_5$r and the various P92 and Y93 variants were prepared at equivalent FAD concentrations (7 $\mu$M) in 10 mM phosphate buffer, containing 0.1 mM EDTA, pH 7.0. Individual spectra correspond to wild type (—), P92A (-○-), Y93A (— — —), Y93F (— — —), Y93H (- - -), Y93W (•••), Y93S (-•-), and Y93D (-••-). Right panel: Oxidized samples of the same c$b_5$r variants in the left panel were prepared at equivalent FAD concentrations (60 $\mu$M) in 10 mM phosphate buffer, containing 0.1 mM EDTA, pH 7.0. Line shapes are the same as those in the left panel. For clarity, the spectra attributed to P92S and P92G are not displayed, but they were similar to that of wild-type c$b_5$r. (B) Visible CD spectra of the Y93A mutant in the absence (- - -) and presence (-•-) of 2 mM 5′-ADP-ribose. Wild-type c$b_5$r alone (—) is shown for comparison.

observed for wild-type c$b_5$r. The Y93W mutant yielded a spectrum with a positive CD maximum occurring at 350 nm that was of decreased intensity compared to that of the corresponding peak in the wild-type spectrum, and a negative CD maximum that remained unshifted but that was of greater intensity than the corresponding peak in the wild-type spectrum, potentially due to a decrease in both solvent exposure and polarity near the isoalloxazine ring. The spectrum of the Y93D mutant was observed to be the most decreased in intensity and resembled that of free FAD. The abnormal spectra obtained for several of the Y93 mutant proteins suggested an increase in solvent exposure of the flavin, either due to the decreased surface area of their side chain substituents, as in Y93A, or the increased hydrophilicity of the side chains themselves, as in Y93H, Y93S, and Y93D.

However, changes in the polarity of the flavin environment were not the only potential cause of the aberrant visible CD spectra. We have previously demonstrated that the visible CD spectrum of c$b_5$r is highly sensitive to the conformation of the protein-bound cofactor (*12*, *23*). In the case of several

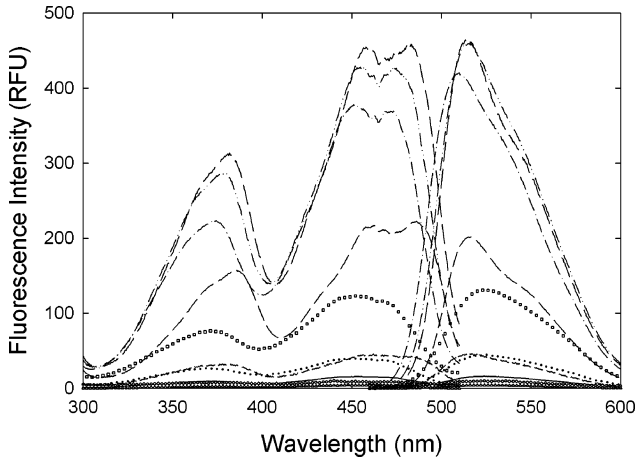


FIGURE 5: Intrinsic flavin fluorescence excitation and emission spectra for the various P92 and Y93 c$b_5$r mutants. Oxidized samples of wild-type c$b_5$r and the different P92 and Y93 variants were prepared at equivalent FAD concentrations (5 $\mu$M) in 10 mM phosphate buffer, containing 0.1 mM EDTA, pH 7.0. Excitation spectra were collected over the wavelength range $\lambda = 300-510$ nm using a constant emission wavelength of 523 nm. Emission spectra were collected over the wavelength range $\lambda = 460-610$ nm using a constant excitation wavelength of 450 nm. Following protein denaturation by boiling, flavin fluorescence measurements were repeated for all the samples and the spectra were normalized to the equivalent residual free flavin fluorescence intensity (□). Normalized, pre-denatured spectra correspond to wild-type c$b_5$r (—), P92A (-○-), P92G (-△-) Y93A (— — —), Y93F (— — —), Y93H (- - -), Y93W (•••), Y93S (-•-), and Y93D (-•••-).

R91-substituted mutants and the type II recessive congenital methemoglobinemia mutant S127P, X-ray diffraction studies have revealed that the displacement of the flavin ADP moiety into the NADH-binding pocket was readily detectable using visible CD. We also demonstrated, using visible CD spectroscopy, that the flavin could be forced into a pseudo-normal conformation within the mutant proteins by addition of the substrate analogues $NAD^+$ and ADP-ribose. Therefore, to determine whether the altered visible CD spectrum of the Y93A variant was the result of a perturbed FAD conformation, similar to that of the R91A variant in which the flavin ADP moiety is displaced toward the NADH-binding lobe (Bewley et al., unpublished) the visible CD spectrum of the Y93A variant was determined in the absence and presence of saturating concentrations of ADP-ribose (Figure 4B). As was previously observed for both selected R91-substituted variants and the S127P mutant, addition of ADP-ribose elicited a change in the visible CD spectrum of the Y93A variant with the resulting spectrum more closely resembling that of the wild-type domain. These results suggested that the Y93A variant exhibited a perturbed flavin conformation which was sensitive to the occupancy of the NADH-binding pocket and that the binding of the substrate analogue ADP-ribose was able to displace the flavin ADP moiety toward a conformation similar to that in the wild-type domain.

The extent of quenching of the intrinsic fluorescence due to the FAD prosthetic group of c$b_5$r has proven to be a sensitive indicator of the retention of the native flavin environment. To probe the flavin fluorescence quenching of the various P92 and Y93 mutants, both excitation and emission fluorescence spectra were recorded prior to and following heat denaturation of the various proteins and are presented in Figure 5. Prior to denaturation, wild-type c$b_5$r, and the P92A, P92S, Y93H, and Y93W variants each quenched the flavin fluorescence to varying degrees ranging from 95% for the wild-type enzyme to only 70% for the Y93H and Y93W variants. Each of the remaining Y93-substituted mutant proteins exhibited enhanced or amplified flavin fluorescence prior to denaturation. The FAD bound within the Y93A, Y93D and Y93S variants was 3.5−4.5 times more fluorescent than free FAD, while an ~1.5-fold enhancement was seen for the Y93F variant. The emission maxima were also blue-shifted to varying extents, as was also observed in the visible absorbance and visible CD spectra, for the Y93A, Y93D, Y93F, Y93H, and Y93S variants.

Previous studies of both free FAD and FMN in solution have revealed that at equivalent concentrations, FMN was approximately nine times more fluorescent than FAD. The decreased intrinsic FAD fluorescence was thought to be due to $\pi-\pi$ stacking interactions between the adenine and isoalloxazine rings of FAD, referred to as the "closed" conformation, that effectively quenched the fluorescence of the flavin (*24*). When FAD was bound within a protein in an extended conformation, the flavin conformation was "opened" and the fluorescence subsequently increased (*24*). That wild-type c$b_5$r quenched the fluorescence of the bound FAD to a greater extent than was seen in the closed conformation, suggested that one or more stacking interactions occur in the protein bound flavin. The excitation and emission spectra obtained for both P92 variants suggested that this residue did not appear to contribute critical stacking interactions with the flavin, since substitution at this position did not alter the extent of flavin fluorescence quenching. However, if Y93 was involved in a stacking interaction with the FAD prosthetic group, as predicted from the X-ray structure of c$b_5$r, nonaromatic substitutions of Y93 with residues such as A, S, or D would be predicted to disturb the quenching of fluorescence. As anticipated, this was experimentally observed for these mutants and the pre-denatured flavin fluorescence intensity was greatly amplified in these variants. It was also anticipated that the Y93W and Y93H variants would quench the intrinsic flavin fluorescence since their side-chain substituents contain either an aromatic ring or a C═C double bond that could contribute to $\pi-\pi$ stacking with the flavin. Similarly, Y93F was expected to effectively quench the flavin fluorescence. However, Y93F exhibited significantly increased fluorescence, corresponding to approximately 1.5-fold that of native c$b_5$r, suggesting the importance of hydrogen bonding in maintaining the correct orientation of the phenol side-chain in the wild-type enzyme, such that stacking interactions occurred to a lesser extent when the phenol moiety was replaced by a benzene ring. These data were in good agreement with the previous findings of Kimura et al. (*14*) that stressed the importance of hydrogen bonding between the tyrosyl-hydroxyl and the 4′-hydroxyl of the flavin ribityl moiety in maintaining the interaction between the isoalloxazine and phenol ring systems.

To examine the influence of the various P92 and Y93 residue substitutions on the stabilities of the resulting proteins, thermal denaturation profiles were generated for wild-type c$b_5$r and each of the mutant proteins by measuring flavin fluorescence emission ($\lambda_{ex} = 450$ nm, $\lambda_{em} = 523$ nm) following incubation of the proteins at temperatures ranging from 0 to 100 °C (Figure 6). For those variants that quenched

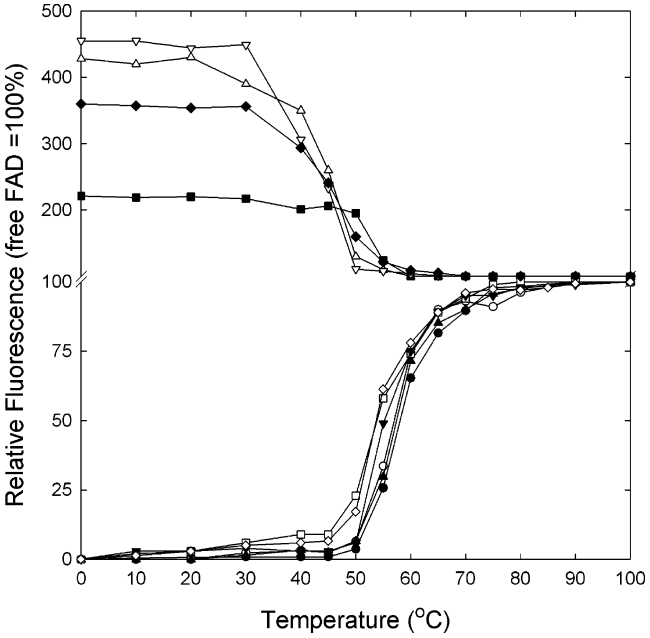


FIGURE 6: Thermal stability profiles for the various P92 and Y93 c$b_5$r mutants. Oxidized samples of wild-type c$b_5$r and the various P92 and Y93 variants (5 $\mu$M FAD) were incubated at the indicated temperatures and aliquots were withdrawn and assayed for intrinsic flavin fluorescence in 10 mM phosphate buffer, containing 0.1 mM EDTA, pH 7.0 using excitation and emission wavelengths of 450 and 523 nm, respectively. The plots correspond to wild-type c$b_5$r (●), P92A (○), P92G (◇), P92S (▲), Y93A (△), Y93F (■), Y93H (□), Y93W (▼), Y93S (▽), and Y93D (◆). Excitation and emission spectra were scaled relative to that of a sample of free FAD (5 $\mu$M) which was assigned a fluorescence intensity of 100%.

the intrinsic fluorescence of the cofactor prior to thermal denaturation, the temperature at which 50% of maximum fluorescence was detected ($T_m$) was an effective indicator of the stability of the core structure of the protein. $T_m$ values increased in the order Y93H > Y93W > P92A > P92S > WT with all variants exhibiting $T_m$ values in the range between 55 and 60 °C, which suggested that none of these substitutions had a dramatic effect on the thermal stability of flavin binding. For the four remaining mutants, Y93A, Y93F, Y93S, and Y93D, fluorescence emission was maximal at low temperature and was observed to decrease to that of free FAD as the temperature was increased, suggesting that flavin release occurred as a result of thermal denaturation, just as was observed with the quenched variants. The Y93F variant exhibited a $T_m$ value of approximately 55 °C, in good agreement with the value obtained for wild-type c$b_5$r. Y93A, Y93S, and Y93D mutants exhibited $T_m$ values that were significantly lower than that of wild-type c$b_5$r, each falling in the range between 40 and 50 °C. These results suggested that substitution of Y93 with alanine, serine, or aspartic acid residues, respectively, adversely influenced the thermal stability of flavin binding, or that the unquenched flavin fluorescence was more sensitive to perturbations in the flavin environment caused by thermal denaturation.

*Enzyme Activities.* As a measure of catalytic efficiency, both NADH:FR, and NADH:BR activities were determined for wild-type c$b_5$r and each of the P92- and Y93-substituted variants, respectively. Kinetic constants derived from these assays are reported in Table 2. With the exception of P92S, which exhibited a slightly elevated activity in the NADH:FR assay, all of the remaining variants exhibited a decreased NADH:FR turnover number compared to that of wild-type c$b_5$r. Specific activities decreased in the order P92S > WT > P92A > P92G > Y93F > Y93A > Y93S > Y93H = Y93D > Y93W with the Y93W mutant retaining only 4% of wild-type NADH:FR activity. The Michaelis constant for NADH utilization increased in the order Y93S > P92A = Y93D > WT > P92G > Y93F > Y93A > P92S > Y93H > Y93W with all variants falling within the range from 4 to 9 $\mu$M, with the exception of Y93W, which exhibited a 9-fold increase ($K_m^{NADH}$ = 54 $\mu$M) compared to wild-type c$b_5$r. The Michaelis constant for the artificial electron acceptor ferricyanide was similar for wild-type c$b_5$r and all of the variants, suggesting that none of the mutations affected either its binding or utilization. The effect of each substitution on the overall NADH:FR catalytic efficiency of the enzyme, reflected in the $k_{cat}/K_m^{NADH}$ value, decreased in the order WT > P92S > P92A > P92G > Y93F > Y93S > Y93A > Y93D > Y93H > Y93W with the least efficient mutant, Y93W, retaining only 0.5% of wild-type c$b_5$r NADH:FR catalytic efficiency.

All of the P92 and Y93 variants were also observed to catalyze the reduction of the physiological electron acceptor, c$b_5$, although with decreased turnover numbers when compared to that of the wild-type domain. NADH:BR $k_{cat}$ values for the c$b_5$r variants were determined to decrease in the order WT > P92G > P92A > P92S > Y93F > Y93A > Y93S > Y93W > Y93D with the least efficient mutant, corresponding to Y93D, retaining only approximately 3% of the activity observed for wild-type c$b_5$r. The Michaelis constant for c$b_5$ was essentially unaffected by any of the P92 or Y93 substitutions, with all values falling within the range from 10 to 15 $\mu$M. $k_{cat}/K_m^{cb5}$ values for the various enzymes decreased in the order WT > P92G > P92A > P92S > Y93F > Y93A > Y93S > Y93W > Y93D, reflecting the decreased turnover numbers. These results suggested that the lower catalytic efficiency observed for the mutants was the result of the decreased affinity for NADH, rather than any decreased affinity for c$b_5$. The kinetic results reinforced the conclusion that P92 was observed to play only a minimal role in modulating c$b_5$r function, while Y93 appeared to have a greater influence on the efficiency of electron transfer through the active site.

*Differential Spectroscopy.* To confirm the effects of the different residue substitutions on the affinities of the various mutants for either NADH or $NAD^+$, spectral binding constants ($K_s$) were determined using differential spectroscopy. Since addition of NADH to either the wild-type enzyme or any of the mutants resulted in efficient bleaching of the flavin visible spectrum, we used the NADH-analogue, 1,4,5,6-tetrahydro-NAD ($H_4$NAD) (*18*) to determine the relative affinities for NADH. $H_4$NAD is a close isosteric analogue of NADH and the interaction with c$b_5$r is assumed to involve a binding conformation similar to that of NADH, due to the neutral charge on its saturated nicotinamide ring, together with the same active site contacts. Previous studies have demonstrated that the NADH-analogue is inactive as an electron donor in either the NADH:FR or NADH:BR assays and does not result in bleaching of the flavin visible absorption spectrum (*17*).

Representative spectra obtained from the titrations of the wild-type enzyme and selected P92 and Y93 variants with

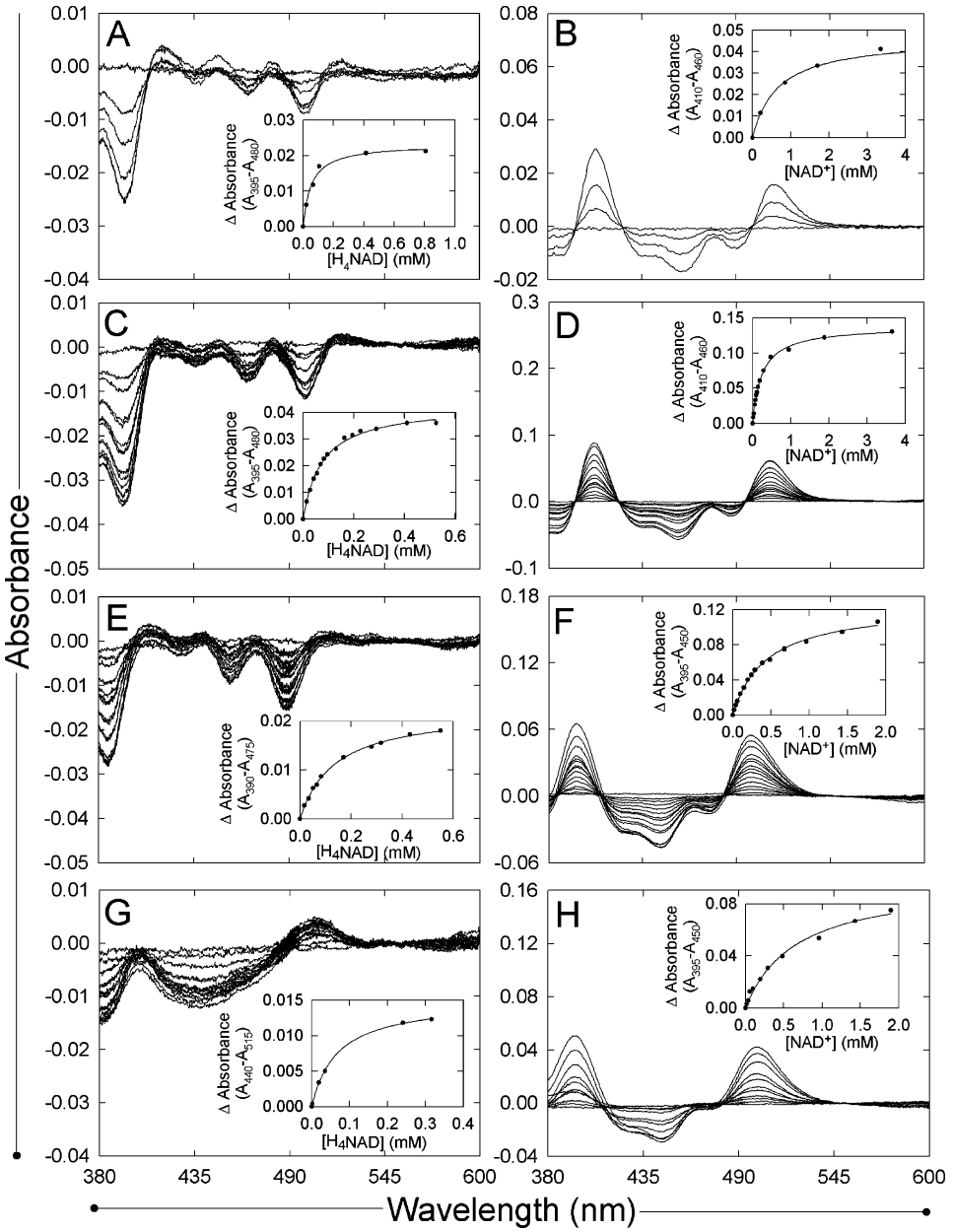


FIGURE 7: Flavin difference spectra obtained following binding of either $H_4NAD$ or $NAD^+$ to wild-type c$b_5$r or the various P92 or Y93 mutants. Difference spectra were obtained for both wild-type c$b_5$r and selected P92 and Y93 mutants at equivalent flavin concentrations (50 $\mu$M FAD) in 20 mM MOPS buffer, containing 0.1 mM EDTA, pH 7.0 following titrations with either $H_4NAD$ (left panels; A, C, E, G) or $NAD^+$ (right panels; B, D, F, H) as described in Materials and Methods. The insert panels correspond to plots of the magnitudes of the observed spectral perturbations (peak to trough measurements at the indicated wavelengths) versus ligand concentration. The corresponding $K_s$ values are given in Table 3.

either $H_4NAD$ or $NAD^+$ are shown in Figure 7. Perturbations of the flavin visible absorbance spectrum were detected for both the wild-type enzyme and all three of the P92 mutants during titrations with $H_4NAD$ and $NAD^+$. However complex formation between either P92A, P92G, or P92S with either $H_4NAD$ or $NAD^+$ produced the same spectral changes, both in terms of the positions of the various difference spectra wavelength maxima and the magnitude of the overall absorbance changes, when compared to the interaction of the wild-type domain with either ligand, suggesting that none of the mutations adversely affected the orientation of either $H_4NAD$ or $NAD^+$ binding. These observations were confirmed by the values obtained for $K_s$, shown in Table 3, for all three P92 variants which were comparable to those obtained for the wild-type domain, indicating that none of the P92 mutations had any significant effect on the affinity for either NADH or $NAD^+$ and reinforcing the results of the multiple sequence alignment that suggested little con-

Table 3. $H_4NAD$ and $NAD^+$ Spectral Binding Constants for the Various P92 and Y93 c$b_5$r Variants

| variant | $K_s^{H_4NAD}$ ($\mu$M) | $K_s^{NAD^+}$ ($\mu$M) |
|---|---|---|
| wild-type | 52 ± 6 | 760 ± 30 |
| P92S | 55 ± 5 | 630 ± 90 |
| P92A | 58 ± 5 | 800 ± 40 |
| P92G | 75 ± 4 | 246 ± 21 |
| Y93F | 62 ± 9 | 2020 ± 100 |
| Y93A | 53 ± 8 | 1290 ± 100 |
| Y93S | 47 ± 5 | 700 ± 50 |
| Y93D | 66 ± 3 | 661 ± 83 |
| Y93H | 143 ± 16 | 438 ± 21 |
| Y93W | 60 ± 10 | 2170 ± 120 |

Table 4. Oxidation−Reduction Midpoint Potentials Obtained for the c$b_5$r FAD/FADH$_2$ Couple ($n = 2$) by Direct Electrochemistry and Dye Equilibration Methods

| | direct electrochemistry | | dye equilibration potentiometry | |
|---|---|---|---|---|
| variant | $E^{\circ\prime}$ [a] (mV) | $\Delta E^{\circ\prime}$ [b] (mV) | $E^{\circ\prime}$ (mV) | $\Delta E^{\circ\prime}$ (mV) |
| wild-type | −232 ± 5 | - | −268 ± 5 | |
| P92S | −233 ± 5 | −1 | −274 ± 5 | −6 |
| P92A | −232 ± 5 | 0 | −278 ± 5 | −10 |
| P92G | −233 ± 5 | −1 | −271 ± 5 | −3 |
| Y93F | −226 ± 5 | +6 | −270 ± 5 | −2 |
| Y93A | −208 ± 5 | +24 | −229 ± 5 | +39 |
| Y93S | −212 ± 5 | +20 | −233 ± 5 | +34 |
| Y93D | −235 ± 5 | −3 | −265 ± 5 | +3 |
| Y93H | −263 ± 5 | −21 | −305 ± 5 | −37 |
| Y93W | −228 ± 5 | +4 | −266 ± 5 | +2 |

[a] Values were determined at 0 mM [$Mg^{2+}$]. [b] $\Delta E^{\circ\prime} = E^{\circ\prime\text{wild-type}} - E^{\circ\prime\text{variant}}$.

servation in the nature of the residue at the second position of the "$RxY^{T}_{S}xx^{S}_{N}$" motif, shown in Figure 1.

However, in contrast to the results obtained for the titrations of the P92 mutants, titrations of the different Y93 variants with either $H_4$NAD or $NAD^+$ revealed altered difference spectra depending on the nature of the amino acid substituent. For the titrations of the various Y93 mutants with $H_4$NAD, the resulting difference spectra could be divided into two classes, as typified by the titrations of the wild-type and Y93S domains, shown in Figure 7. For the first class, which consisted of the titrations of the wild-type domain and the Y93A, Y93F, and Y83W mutants, similar difference spectra were observed that could be identified by the positions of the weak positive absorbance maxima at approximately 420, 450, and 481 nm, respectively, and the strong negative absorbance maxima at 395, 467, and 500 nm, while the second class comprised the Y93S titration that was identified by strong positive transitions at 405 and 510 nm and a strong negative absorption maximum at 455 nm. These results suggested that binding of $H_4$NAD to the wild-type domain and the Y93A, Y93F, and Y93W mutants resulted in a conserved geometry with respect to the flavin isoalloxazine ring while the binding of $H_4$NAD to the Y93S variant resulted in a significantly different interaction between the ligand and the FAD. The corresponding titrations of the Y93 variants, however, revealed essentially identical difference spectra suggesting that $NAD^+$ bound with a similar geometry both to the wild-type domain and the Y93A, F, W, and S mutants.

The corresponding $K_s$ values obtained for the various titrations, given in Table 3, revealed that the Y93F and W substitutions resulted in a somewhat decreased affinity for $H_4$NAD when compared to either the wild-type domain or the Y93A and S variants, respectively. Similarly, for the $NAD^+$ titrations, only the Y93F and W variants showed markedly decreased affinity for $NAD^+$.

*Flavin Oxidation−Reduction Potentials.* To examine the effects of the various amino acid substitutions on the thermodynamic properties of the FAD prosthetic group, oxidation−reduction midpoint potentials were determined for the FAD/FADH$_2$ couple ($E^{\circ\prime}$, $n = 2$) in wild-type c$b_5$r and each of the P92 and Y93 variants using both direct voltammetry and dye-equilibration potentiometric methods. $E^{\circ\prime}$ values obtained by both methods for the FAD/FADH$_2$ couple in the various mutants are compared in Table 4. The flavin midpoint potentials as determined by direct electrochemistry, were consistent for wild-type c$b_5$r and the P92A, P92G, Y93F, Y93W, and Y93D variants and were within the estimated ±5 mV error range of the measurements. Two mutants, Y93A and Y93S, exhibited flavin $E^{\circ\prime}$ values that were 24 and 20 mV, respectively, more positive than that of the wild-type enzyme, while the $E^{\circ\prime}$ of the Y93H mutant was 21 mV more negative than that of wild-type c$b_5$r. The potential of the P92S mutant could not be determined due to the aggregation of this variant at the elevated protein concentration required for analysis using direct electrochemistry and the extensive time required for the xanthine/xanthine oxidase titrations which resulted in extensive light scattering and spectral degradation. However, comparison of the results obtained for the wild-type enzyme and the remaining eight mutants confirmed that Y93 played a significant role in modulating the oxidation−reduction midpoint potential of the FAD prosthetic group of c$b_5$r.

To confirm the results of the direct electrochemical determinations, midpoint potentials for the FAD/FADH$_2$ couple were also determined for each mutant by dye equilibration potentiometry using phenosafranine as a redox indicator. Representative spectra obtained during the redox titration of the P92A mutant are shown in Figure 8A, and provide an example of the nature of the spectral changes observed during the dye-equilibration redox titrations while the corresponding Nernst plots for the wild-type and selected mutants are presented in Figure 8B. The standard midpoint potentials ($E^{\circ\prime}$) obtained for the FAD/FADH$_2$ couple ($n = 2$) from the various potentiometric analyses are listed in Table 4. The redox potentials of the P92A, P92G, Y93F, Y93W, and Y93D variants were all within 10 mV of wild-type c$b_5$r, suggesting that these mutations had little effect on the thermodynamic properties of the FAD prosthetic group. However, in contrast, the Y93A and Y93S variants were 39 mV and 34 mV more positive than wild-type c$b_5$r, respectively, whereas the Y93H variant was 37 mV more negative than wild-type c$b_5$r. The general trend in $\Delta E^{\circ\prime}$ values for these mutants was consistent with those obtained through direct voltammetry, although in most cases, the direct voltammetry measurements yielded midpoint potentials that were approximately 20−30 mV more positive than the values obtained from the dye equilibration studies. The slopes of the various Nernst plots were within the range −30 ± 3 mV for all the mutants examined with the exception of the Y93W variant which exhibited a slope of −40 mV, suggesting that for this variant, there was some deviation from the normal wild-type $n = 2$ redox behavior which may reflect an increase in the separation between the FAD/FAD$^{\bullet-}$ and the FAD$^{\bullet-}$/FADH$_2$ redox couples.

The oxidation−reduction midpoint potential ($n = 2$) determined by dye equilibration for the FAD/FADH$_2$ couple in wild-type c$b_5$r was −268 mV, a value in good agreement with the −258 mV potential previously reported by Iyanagi (*25*) for the porcine enzyme, which was determined via dithionite titration in the presence of various dye mediators. However, the $E^{\circ\prime}$ of wild-type c$b_5$r as determined by direct voltammetry was −232 mV, a difference of 36 mV. Despite the apparent discrepancy in absolute potentials, the relative differences in the potentials obtained for the Y93A, Y93H, and Y93S variants compared to wild-type c$b_5$r were in

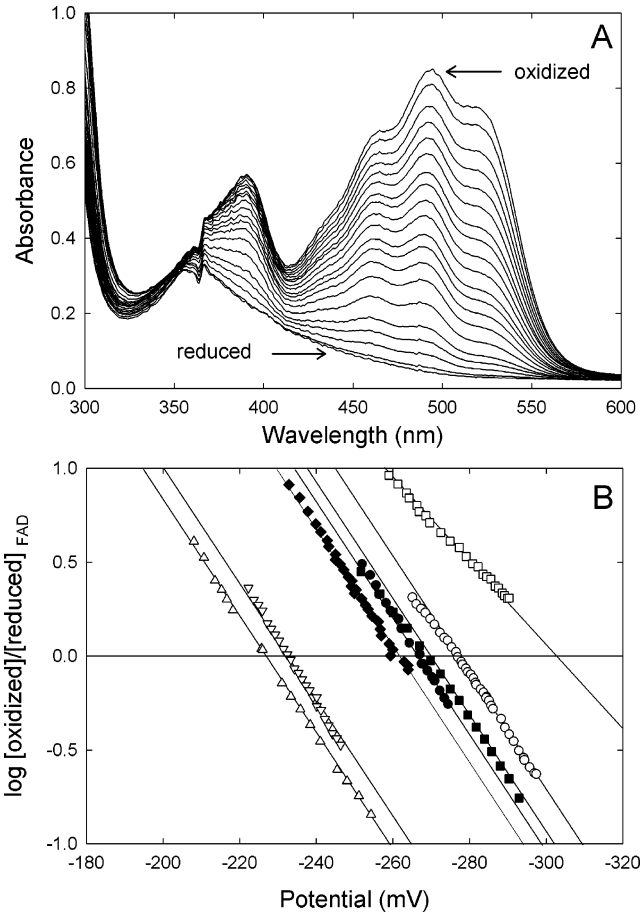


FIGURE 8: Oxidation−reduction midpoint potentials for the FAD prosthetic group in c$b_5$r and selected P92 and Y93 mutants. Reductive dye-equilibration titrations of wild-type and the different P92 and Y93 variants of c$b_5$r (40 $\mu$M FAD) were performed as described under Materials and Methods in 100 mM phosphate buffer, containing 0.1 mM EDTA, pH 7.0 in the presence of phenosafranine (15 $\mu$M, $E^{\circ\prime} = -252$ mV) (*20*). Individual spectra were collected at 2−3 min intervals during the time course of the titrations. A. Selected spectra obtained during the dye-mediated redox titration of the P92A variant in the presence of phenosafranine are shown with the initial oxidized and final reduced spectra labeled. B. The corresponding Nernst plots obtained for the FAD/$FADH_2$ couple ($n = 2$) are shown for the titrations of the various P92 and Y93 mutants and correspond to wild-type c$b_5$r (●), P92A (○), Y93A (△), Y93F (■), Y93W (●), Y93H (□), Y93S (▽), and Y93D (◆).

relative agreement and suggested that substitution of Y93 had a significant impact on the overall flavin redox potential.

## DISCUSSION

The preceding results provide the first detailed comparison of the spectroscopic, kinetic and thermodynamic properties of a series of mutations that target both the second and third residues within the "$RxY^{T}_{S}xx^{S}_{N}$" (R91−S97) sequence motif present in the diaphorase domain of rat c$b_5$r, a seven-residue functional motif that has been shown to be conserved in all members of the FNR superfamily of flavoprotein transhydrogenases.

As anticipated, the biophysical properties of the three P92 mutants were relatively unchanged from those of the wild-type c$b_5$r flavin domain which is in agreement with the lack of sequence conservation at this position in the signature motif. In the structure of rat c$b_5$r (*7*), P92 forms part of the hydrophobic surface against which the *si*-face of the isoalloxazine portion of the flavin cofactor stacks. Although the distance separating the $\gamma$-carbon of the proline side-chain and the flavin N10 atom is only 5.14 Å in the wild-type domain, replacement of the proline side chain by either a nonpolar methyl group or a polar hydroxyl function or effective removal of the side chain via a glycine substitution, had no significant adverse effects on either the extent of FAD incorporation, overall domain folding and either the spectroscopic or thermodynamic properties of the flavin prosthetic group. In addition, the A, S and G substitutions had only modest impact on either the NADH:FR or NADH:BR catalytic efficiencies with little change in the affinities for either NADH or $NAD^+$, indicating that this residue plays only a minor structural or functional role. Substitution of P92 by glycine was observed to have the most significant effect of the three P92 mutations on NADH:FR activity resulting in an ~40% decrease in activity. Within the three-dimensional structure of the rat c$b_5$r flavin domain (PDB = 1I7P), P92 has been shown to make a number of side chain hydrophobic contacts with the flavin isoalloxazine ring while the backbone carbonyl oxygen is hydrogen-bonded to the O2 atom of the ribityl moiety (*7*). However, multiple sequence alignments have revealed that within c$b_5$r homologues , residue 92 can be identified as either a proline, alanine or serine residue while within other FNR superfamily members, a more diverse range of amino acid residues, including tyrosine, cysteine and leucine, are tolerated at this position, although the general trend is for the presence of an aliphatic hydrocarbon side chain in the majority of the FNR family sequences. While a glycine residue at position 92 has not be observed in any c$b_5$r homologue or any other member of the FNR superfamily, we chose to construct the P92G variant since glycine residues have been shown to have the greatest variation in backbone $\phi-\psi$ angles and thus would be expected to result in peptide backbone perturbation according to $\phi-\psi$ angle predictions. The glycine residue essentially lacks a side chain which can confer a high degree of local flexibility to the polypeptide chain. Thus, the P92G variant would be the only mutant in which alterations in the backbone structure could potentially result in loss of the hydrogen-bond between the carbonyl oxygen atom and the O2 atom of the FAD ribityl moiety. While the results obtained for the P92G variant revealed a significant decrease in NADH:FR activity and the $K_s$ for $NAD^+$ binding, no corresponding alterations in the FAD/$FADH_2$ redox couple were observed. However, overall, the P92 A, S and G mutants functioned as appropriate and valuable controls for assessing the general effects of altering the side-chain substituents or replacing noncritical amino acid residues within the "$RxY^{T}_{S}xx^{S}_{N}$" sequence motif.

In contrast to the results observed following the substitution of P92 on the properties of rat c$b_5$r, altering the nature of the side chain substituent at residue 93, the third residue in the motif sequence, had a profound effect on both the structure and catalytic efficiency of the diaphorase domain.

Spectroscopically, substituting the tyrosine residue with either phenylalanine or tryptophan, a strategy that was designed to conserve the aromatic character of the side chain while removing the side chain hydrogen-bonding capacity, resulted in only minor alterations in the visible absorbance spectra of the proteins, although the visible CD spectra showed greater deviation from the wild-type line shape,

particularly for the Y93W variant. In addition, comparison of the spectra obtained for the Y93A variant, suggested that while loss of the side-chain hydrogen bond to the ribityl moiety had little effect, the loss of aromaticity greatly influenced the spectral properties of the FAD prosthetic group. These results were also reflected in the changes in the oxidation−reduction potentials obtained for the FAD/$FADH_2$ couple in the various mutants. The flavin redox potential was unaffected by either the phenylalanine or tryptophan substitutions, but was elevated approximately 40 mV by the alanine substitution.

For rat c$b_5$r, substitution of phenylalanine for tyrosine at residue 93 would be anticipated to result in abolition of the phenol hydroxyl-4′ ribityl hydrogen bond but with retention of the aromatic interaction with the flavin isoalloxazine ring. Our studies demonstrated that deletion of the hydrogen bond adversely affected the catalytic efficiency of the enzyme with an approximately 40% decrease in $k_{cat}$ for the NADH:FR activity with no associated decrease in the affinity for the reducing substrate, NADH. This result is in agreement with our structural studies of the wild-type domain that have demonstrated that the majority of contacts involved in regulating affinity for the pyridine nucleotides are present in the NADH/$NAD^+$ -binding lobe opposite the *re*-face of the FAD prosthetic group (*7*).

Substitution of an indole moiety for the phenol group in the Y93W variant was found to have the most significant impact on the c$b_5$r catalytic activity. In this mutant, both NADH:FR and NADH:BR activities were decreased to ∼5% of the wild-type value.

Arakaki et al. have performed *ab initio* molecular orbital calculations of free energy versus phenol-lumiflavin angle and free energy versus phenol-lumiflavin distance for a variety of flavoproteins containing a tyrosine near the *si*-face of the isoalloxazine ring (*26*). Their calculations suggested that the most energetically favorable orientation between the two ring systems occurred at a distance of 4.6 Å and at an angle of 54°. The crystal structures of several FNR family flavoproteins including c$b_5$r (*7*), FNR (*27*), NR (*28*), PDR (*8*), and CYPOR (*29*) place the phenol side-chain of the conserved tyrosine residue of the "$RxY^T_Sxx^S_N$" motif (equivalent to Y93 of rat c$b_5$r) within 5 Å of the cofactor N1 and N5 atoms, where the planes of the two ring systems intersect at an approximate 50° angle. Superposition of the structures in Figure 1C showed the similarity in orientation of the flavin cofactor and conserved tyrosine in each of the proteins. This orientation suggests that the phenol ring is involved in $\pi-\pi$ interactions with the isoalloxazine ring, while a hydrogen bond is formed between the 4′-hydroxyl of the flavin ribityl moiety and the phenolic hydroxyl of the tyrosine residue.

Limited studies of two mutants of the identical residue in porcine c$b_5$r, corresponding to Y65A and Y65F, by Kimura et al. (*11*) suggested that maintenance of the aromatic interaction, tethered through hydrogen-bonding, contributed to both the affinity for FAD and the overall stability of the diaphorase domain while the decreased mutant activities were a result of impaired shielding of the isoalloxazine ring from the solvent. Our results are in general agreement with these studies. Both the NADH:FR and intrinsic flavin fluorescence $T_m$ studies indicated that while the various P92 mutations had no significant impact on domain stability, the Y93 variants were all less stable than wild-type c$b_5$r. Similar results were obtained for our prior studies of various c$b_5$r R91 mutants (*12*), however, substitution of R91 resulted in several mutants that were more unstable than the Y93 variants suggesting that R91 may play a greater role in modulating the affinity for the flavin cofactor than Y93.

The magnitude of the changes in the oxidation−reduction midpoint potential of the FAD/$FADH_2$ couple ($n = 2$) in some of the Y93-substituted variants, such as the ∼ +40 mV shift for Y93A and S and the ∼ −40 mV shift for Y93H, has confirmed that interactions between the side-chain atoms of Y93 and the flavin isoalloxazine ring are potentially significant contributors to the modulation of the thermodynamic properties of the FAD prosthetic group in c$b_5$r, whereas, in contrast, substitution of P92 had no impact on the FAD potential. Chang et al. (*30*) have suggested that hydrogen bonding to the phospho-ribityl moiety of the FMN cofactor of flavodoxin was critical to maintaining the flavin midpoint potential. However, since the Y93F variant would be expected to lack the hydrogen bond with the 4′ ribityl of the FMN portion of the FAD in c$b_5$r, our results suggest that hydrogen bond interactions with the flavin ribityl moiety do not appreciably regulate the flavin midpoint potential.

The results obtained from probing the effects of the various c$b_5$r Y93 substitutions can be contrasted with previous data obtained from mutagenesis of the corresponding residue in pea FNR (Y89) (*26*) which indicated that aromaticity on residue 89 was essential for FAD binding and correct protein folding. While the Y89F and Y89W variants could be generated, although with decreased levels of FAD incorporation, protein stability and associated catalytic activity, the latter corresponding to 39% and 0.4% of wild-type values, respectively, two variants corresponding to Y89S and Y89G could not be obtained as purified proteins suggesting that the active site of FNR was significantly less-tolerant of side chain substitutions at this position than c$b_5$r.

Our studies suggest that alterations in the relatively nonconserved residues in the "$RxY^T_Sxx^S_N$" flavin binding motif have little impact on either the physicochemical properties of the FAD prosthetic group or the catalytic efficiency of the enzyme. However, changes in the nature of the side-chain substituents in the conserved residues, such as R91 and Y93, exert considerable influence on the properties of the flavin prosthetic group and significantly impact c$b_5$r turnover confirming that these residues are critical to both FAD binding and positioning and to maintaining the correct architecture of the catalytic site and the orientation of bound pyridine nucleotides. The results obtained for c$b_5$r may provide additional general insight into the effects of similar substitutions in other members of the FNR family of flavoprotein transhydrogenases.

## ACKNOWLEDGMENT

We thank Michael A. Bahe for his assistance in the preparation of some of the mutant enzymes and assistance with the initial studies.

## REFERENCES

1. Strittmatter, P. (1962) Direct hydrogen transfer from reduced pyridine nucleotides to microsomal cytochrome b5 reductase, *J. Biol. Chem. 237*, 3250−3254.

2. Hultquist, D. E., and Passon, P. G. (1971) Catalysis of methaemoglobin reduction by erythrocyte cytochrome B5 and cytochrome B5 reductase, *Nat. New Biol. 229*, 252−254.
3. Keyes, S. R., and Cinti, D. L. (1980) Biochemical properties of cytochrome b5-dependent microsomal fatty acid elongation and identification of products, *J. Biol. Chem. 255*, 11357−11364.
4. Strittmatter, P., Spatz, L., Corcoran, D., Rogers, M. J., Setlow, B., and Redline, R. (1974) Purification and properties of rat liver microsomal stearyl coenzyme A desaturase, *Proc. Natl. Acad. Sci. U.S.A. 71*, 4565−4569.
5. Hildebrandt, A., and Estabrook, R. W. (1971) Evidence for the participation of cytochrome b 5 in hepatic microsomal mixed-function oxidation reactions, *Arch. Biochem. Biophys. 143*, 66−79.
6. Reddy, V. V., Kupfer, D., and Caspi, E. (1977) Mechanism of C-5 double bond introduction in the biosynthesis of cholesterol by rat liver microsomes, *J. Biol. Chem. 252*, 2797−2801.
7. Bewley, M. C., Marohnic, C. C., and Barber, M. J. (2001) The structure and biochemistry of NADH-dependent cytochrome b5 reductase are now consistent, *Biochemistry 45*, 13574−13582.
8. Correll, C. C., Batie, C. J., Ballou, D. P., and Ludwig, M. L. (1992) Phthalate dioxygenase reductase: a modular structure for electron transfer from pyridine nucleotides to [2Fe-2S], *Science 258*, 1604−1610.
9. Nishida, H., Inaka, K., Yamanaka, M., Kaida, S., Kobayashi, K., and Miki, K. (1995) Crystal structure of NADH-cytochrome b5 reductase from pig liver at 2.4 A resolution, *Biochemistry 34*, 2763−2767.
10. Nishida, H., Inaka, K., and Miki, K. (1995) Specific arrangement of three amino acid residues for flavin-binding barrel structures in NADH-cytochrome b5 reductase and the other flavin-dependent reductases, *FEBS Lett. 361*, 97−100.
11. Kimura, S., Hirokazu, N., and Iyanagi, T. (2001) Effects of flavin-binding motif amino acid mutations in the NADH-cytochrome b5 reductase catalytic domain on protein stability and catalysis, *J. Biochem. (Tokyo) 130*, 481−490.
12. Marohnic, C. C., and Barber, M. J. (2001) Arginine 91 is not essential for flavin incorporation in hepatic cytochrome b(5) reductase, *Arch. Biochem. Biophys. 389*, 223−233.
13. Marohnic, C. C., Davis, C. A., Bewley, M. C., and Barber, M. J. (2002) Flavin flexibility in cytochrome $b_5$ reductase, *FASEB J. 16*, 10.
14. Kimura, S., Kawamura, M., and Iyanagi, T. (2003) Role of Thr-(66) in porcine NADH-cytochrome b5 reductase in catalysis and control of the rate-limiting step in electron transfer, *J. Biol. Chem. 278*, 3580−3589.
15. Beck-von Bodman, S. B., Schuler, M. A., Jollie, D. R., and Sligar, S. G. (1986) Synthesis, bacterial expression, and mutagenesis of the gene coding for mammalian cytochrome b5, *Proc. Natl. Acad. Sci. U.S.A. 83*, 9443−9447.
16. Laemmli, U. K. (1970) Cleavage of structural proteins during the assembly of the head of bacteriophage T4, *Nature 227*, 680−685.
17. Marohnic, C. C., Bewley, M. C., and Barber, M. J. (2003) Engineering and characterization of a NADPH-utilizing cytochrome b5 reductase, *Biochemistry 42*, 11170−11182.
18. Murataliev, M. B., and Feyereisen, R. (2000) Interaction of NADP(H) with oxidized and reduced P450 reductase during catalysis. Studies with nucleotide analogues, *Biochemistry 39*, 5066−5074.
19. Trimboli, A. J., Quinn, G. B., Smith, E. T., and Barber, M. J. (1996) Thiol modification and site directed mutagenesis of the flavin domain of spinach NADH:nitrate reductase, *Arch. Biochem. Biophys. 331*, 117−126.
20. Massey, V. (1991) A simple method for the determination of redox potentials, *Flavin and Flavoproteins 1990* (B. Curti, S. Ronchi and G. Zanetti editors), de Gruyter, Berlin, 59−66.
21. Müller, F. (1991) Free flavins: syntheses, chemical and physical properties, *Chemistry and Biochemistry of Flavoenzymes Vol. 1*, (F. Müller editor), CRC Press, Boca Raton, 1-60.
22. Kuchler, B., Abdel-Ghany, A. G., Bross, P., Nandy, A., Rasched, I., and Ghisla, S. (1999) Biochemical characterization of a variant human medium-chain acyl-CoA dehydrogenase with a disease-associated mutation localized in the active site, *Biochem. J. 337*, 225−230.
23. Bewley, M. C., Davis, C. A., Marohnic, C. C., Tormina, D., and Barber, M. J. (2003) The structure of the S127P mutant of cytochrome b5 reductase that causes methemoglobinemia shows the AMP moiety of the flavin occupying the substrate binding site, *Biochemistry 42*, 13145−13151.
24. van den Berg, P. A., Widengren, J., Hink, M. A., Rigler, R., and Visser, A. J. (2001) Fluorescence correlation spectroscopy of flavins and flavoenzymes: photochemical and photophysical aspects, *Spectrochim. Acta A. Mol. Biomol. Spectrosc. 57*, 2135−2144.
25. Iyanagi, T. (1977) Redox properties of microsomal reduced nicotinamide adenine dinucleotide-cytochrome b5 reductase and cytochrome b5, *Biochemistry 16*, 2725−2730.
26. Arakaki, A. K., Orellano, E. G., Calcaterra, N. B., Ottado, J., and Ceccarelli, E. A. (2001) Involvement of the flavin si-face tyrosine on the structure and function of ferredoxin-NADP$^+$ reductases, *J. Biol. Chem. 276*, 44419−44426.
27. Karplus, P. A., Daniels, M. J., and Herriott, J. R. (1991) Atomic structure of ferredoxin-NADP+ reductase: prototype for a structurally novel flavoenzyme family, *Science 251*, 60−66.
28. Lu, G., Lindqvist, Y., Schneider, G., Dwived, U., and Campbell, W. (1995) Structural studies on corn nitrate reductase: refined structure of the cytochrome b reductase fragment at 2.5 A, its ADP complex and an active-site mutant and modeling of the cytochrome b domain, *J. Mol. Biol. 248*, 931−948.
29. Wang, M., Roberts, D. L., Paschke, R., Shea, T. M., Masters, B. S., and Kim, J. J. (1997) Three-dimensional structure of NADPH-cytochrome P450 reductase: prototype for FMN- and FAD-containing enzymes, *Proc. Natl. Acad. Sci. U.S.A. 94*, 8411−8416.
30. Chang, F. C., Bradley, L. H., and Swenson, R. P. (2001) Evaluation of the hydrogen bonding interactions and their effects on the oxidation−reduction potentials for the riboflavin complex of the *Desulfovibrio vulgaris* flavodoxin, *Biochim. Biophys. Acta 1504*, 319−328.
31. Hermoso, J. A., Mayoral, T., Faro, M., Gomez-Moreno, C., Sanz-Aparicio, J., and Medina, M. (2002) Mechanism of coenzyme recognition and binding revealed by crystal structure analysis of ferredoxin-NADP$^+$ reductase complexed with NADP$^+$, *J. Mol. Biol. 319*, 1133−1142.
32. Pietrini, G., Carrera, P., and Borgese, N. (1988) Two transcripts encode rat cytochrome b5 reductase, *Proc. Natl. Acad. Sci. U.S.A. 85*, 7246−7250.
33. Shiraishi, N., Kubo, Y., Takeba, K., Kiyota, S., Sakano, K., and Nakagawa, H. (1991) Sequence analysis of cloned cDNA and proteolytic fragments for nitrate reductase from *Spinacia oleracea*, *Plant Cell Physiol. 32*, 1031−1038.
34. Newman, B. J., and Gray, J. C. (1988) Characterization of a full-length cDNA clone for pea ferredoxin-NADP$^+$ reductase, *Plant Mol. Biol. 10*, 511−520.
35. Haniu, M., McManus, M. E., Birkett, D. J., Lee, T. D., and Shively, J. E. (1989) Structural and functional analysis of NADPH-cytochrome P-450 reductase from human liver: complete sequence of human enzyme and NADPH-binding sites, *Biochemistry 28*, 8639−8645.
36. Nakane, M., Schmidt, H. H., Pollock, J. S., Forstermann, U., and Murad, F. (1993) Cloned human brain nitric oxide synthase is highly expressed in skeletal muscle, *FEBS Lett. 316*, 175−180.
37. Nomura, Y., Nakagawa, M., Ogawa, N., Harashima, S., and Oshima, Y. (1992) Genes in PHT plasmid encoding the initial degradation pathway of phthalate in *Pseudomonas putida*, *J. Ferment. Bioeng. 74*, 333−344.
38. Leclerc, D., Wilson, A., Dumas, R., Gafuik, C., Song, D., Watkins, D., Heng, H. H., Rommens, J. M., Scherer, S. W, Rosenblatt, D. S., and Gravel, R. A. (1998) Cloning and mapping of a cDNA for methionine synthase reductase, a flavoprotein defective in patients with homocystinuria, *Proc. Natl. Acad. Sci. U.S.A. 95*, 3059−3064.
39. Ostrowski, J., Wu, J. Y., Rueger, D. C., Miller, B. E., Siegel, L. M., and Kredich, N. M. (1989) Characterization of the cysJIH regions of *Salmonella typhimurium* and *Escherichia coli* B. DNA sequences of cysI and cysH and a model for the siroheme-Fe4S4 active center of sulfite reductase hemoprotein based on amino acid homology with spinach nitrite reductase, *J. Biol. Chem. 264*, 15726−15737.
40. Plamann, M. D., and Stauffer, G. V. (1983) Characterization of the *Escherichia coli* gene for serine hydroxymethyltransferase, *Gene 22*, 9−18.
41. Davis, C. A., Dhawan, I. K., Johnson, M. K., and Barber, M. J. (2002) Heterologous expression of an endogenous rat cytochrome b(5)/cytochrome b(5) reductase fusion protein: identification of histidines 62 and 85 as the heme axial ligands, *Arch. Biochem. Biophys. 400*, 63−75.
42. Bosch, R., Garcia-Valdes, E., and Moore, E. R. (1999) Genetic characterization and evolutionary implications of a chromosomally

encoded naphthalene-degradation upper pathway from *Pseudomonas stutzeri* AN10, *Gene 1*, 149−157.
43. Nordlund, I., Powlowski, J., and Shingler, V. (1990) Complete nucleotide sequence and polypeptide analysis of multicomponent phenol hydroxylase from *Pseudomonas* sp. strain CF600, *J. Bacteriol. 172*, 6826−6833.
44. Welch, R. A., Burland, V., Plunkett, G., 3rd, Redford, P., Roesch, P., Rasko, D., Buckles, E. L., Liou, S. R., Boutin, A., Hackett, J., Stroud, D., Mayhew, G. F., Rose, D. J., Zhou, S., Schwartz, D. C., Perna, N. T., Mobley, H. L., Donnenberg, M. S., and Blattner, F. R. (2002) Extensive mosaic structure revealed by the complete genome sequence of uropathogenic *Escherichia coli*, *Proc. Natl. Acad. Sci. U.S.A. 99*, 17020−17024.
45. Jiang, X. M., Neal, B., Santiago, F., Lee, S. J., Romana, L. K., and Reeves, P. R. (1991) Structure and sequence of the rfb (O antigen) gene cluster of *Salmonella serovar typhimurium* (strain LT2), *Mol. Microbiol. 5*, 695−713.
46. Eaton, R. W. (1996) p-Cumate catabolic pathway in *Pseudomonas putida* Fl: cloning and characterization of DNA carrying the cmt operon, *J. Bacteriol. 178*, 1351−1362.
47. James, K. D., and Williams, P. A. (1998) ntn genes determining the early steps in the divergent catabolism of 4-nitrotoluene and toluene in *Pseudomonas* sp. strain TW3, *J. Bacteriol. 180*, 2043−2049.
48. Rosche, B., Tshisuaka, B., Hauer, B., Lingens, F., and Fetzner, S. (1997) 2-oxo-1,2-dihydroquinoline 8-monooxygenase: phylogenetic relationship to other multicomponent nonheme iron oxygenases, *J. Bacteriol. 179*, 3549−3554.
49. Stainthorpe, A. C., Lees, V., Salmond, G. P., Dalton, H., and Murrell, J. C. (1990) The methane monooxygenase gene cluster of *Methylococcus capsulatus* (Bath), *Gene 91*, 27−34.
50. Bundy, B. M., Campbell, A. L., and Neidle, E. L. (1998) Similarities between the antABC-encoded anthranilate dioxygenase and the benABC-encoded benzoate dioxygenase of *Acinetobacter* sp. strain ADP1, *J. Bacteriol. 180*, 4466−4474.
51. Neidle, E. L., Hartnett, C., Ornston, L. N., Bairoch, A., Rekik, M., and Harayama, S. (1991) Nucleotide sequences of the *Acinetobacter calcoaceticus* benABC genes for benzoate 1,2-dioxygenase reveal evolutionary relationships among multicomponent oxygenases, *J. Bacteriol. 173*, 5385−5395.
52. Haak, B., Fetzner, S., and Lingens, F. (1995) Cloning, nucleotide sequence, and expression of the plasmid-encoded genes for the two-component 2-halobenzoate 1,2-dioxygenase from *Pseudomonas cepacia* 2CBS, *J. Bacteriol. 177*, 667−675.
53. Kalman, S., Mitchell, W., Marathe, R., Lammel, C., Fan, J., Hyman, R. W., Olinger, L., Grimwood, J., Davis, R. W., and Stephens, R. S. (1999) Comparative genomes of *Chlamydia pneumoniae* and *C. trachomatis*, *Nat. Genet. 21*, 385−389.
54. Kaneko, T., Nakamura, Y., Sato, S., Asamizu, E., Kato, T., Sasamoto, S., Watanabe, A., Idesawa, K., Ishikawa, A., Kawashima, K., Kimura, T., Kishida, Y., Kiyokawa, C., Kohara, M., Matsumoto, M., Matsuno, A., Mochizuki, Y., Nakayama, S., Nakazaki, N., Shimpo, S., Sugimoto, M., Takeuchi, C., Yamada, M., and Tabata, S. (2000) Complete genome structure of the nitrogen-fixing symbiotic bacterium *Mesorhizobium loti*, *DNA Res. 7*, 331−338.
55. Ng, W. V., Kennedy, S. P., Mahairas, G. G., Berquist, B., Pan, M., Shukla, H. D., Lasky, S. R., Baliga, N. S., Thorsson, V., Sbrogna, J., Swartzell, S., Weir, D., Hall, J., Dahl, T. A., Welti, R., Goo, Y. A., Leithauser, B., Keller, K., Cruz, R., Danson, M. J., Hough, D. W, Maddocks, D. G., Jablonski, P. E., Krebs, M. P., Angevine, C. M., Dale, H., Isenbarger, T. A., Peck, R. F., Pohlschroder, M., Spudich, J. L., Jung, K. W., Alam, M., Freitas, T., Hou, S., Daniels, C. J., Dennis, P. P., Omer, A. D., Ebhardt, H., Lowe, T. M., Liang, P., Riley, M., Hood, L., and DasSarma, S. (2000) Genome sequence of *Halobacterium* species NRC-1, *Proc. Natl. Acad. Sci. USA 97*, 12176−12181.
56. Zhou, N. Y., Jenkins, A., Chan Kwo Chion, C. K., and Leak, D. J. (1999) The alkene monooxygenase from *Xanthobacter* strain Py2 is closely related to aromatic monooxygenases and catalyzes aromatic monohydroxylation of benzene, toluene, and phenol, *Appl. Environ. Microbiol. 65*, 1589−1595.

BI048045Q